Chapter 3

Functionalized Thermoplastic Polyurethane Gel Electrolytes for Cosensitized TiO_2/CdS/CdSe Photoanode Solar Cells with High Efficiency

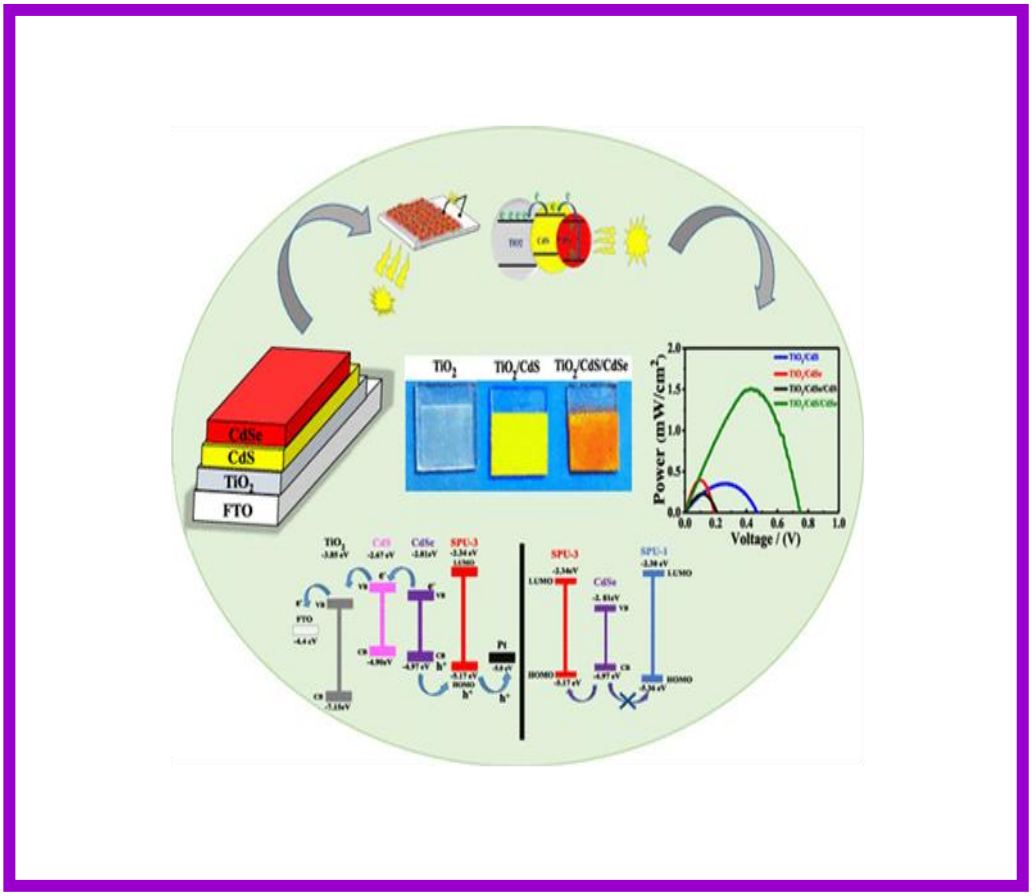

Energy & Fuels. (2020);34: 16847-16857

3.1 Introduction

Global warming associated with water and air pollution during the production of conventional energy from fossil fuels (coal, oil and natural gas) demand a green and clean energy globally.[117] Renewable energy resources have great importance for the clean energy demands. The conversion of sun light in to electrical energy through photoelectric effect is being used currently by fabricating a device, known as solar cell. An hour of sun light reaches on earth is equivalent to 4.3×10^{20} J which is sufficient to fulfill the energy need (4.1×10^{20} J) of whole world for a year.[117] To cater the partial demand of energy, a variety of solar cell has been developed and a lot more research is going on the solar energy technology. The third-generation solar cell consists of various technologies *e.g.,* solar cells sensitized by organic dye, sensitized by quantum dots and/or perovskite-sensitized solar cells. These types of solar cells have attracted great attention recently because of its easy fabrication process and high photo conversion efficiency. The third-generation solar cell is made of photoanode, charge transport medium *i.e.,* electrolytes and a counter electrode. When the QDs are deposited on wide band gap semiconductor like TiO_2, QDs have the ability to transfer the excited electron to the conduction band of wide band gap semiconductor. Inorganic semiconductors (quantum dots) are used as light absorbing materials instead of organic dyes in solar cells to generate exciton, known as quantum dots sensitized solar cells (QDSSC). The theoretical efficiency of QDSSCs, calculated by considering carrier multiplication due to impact of ionization, was found to be 44%.

Electrolyte plays an important role in QDSSCs, which accept the holes from the valence band of QDs and transfer it to the counter electrode to complete the circuit. Electrolytes are of three types, liquid, quasi-liquid and solid-state electrolytes depending upon their physical states. The most common liquid electrolytes used in QDSSCs are I^-/I_3^- and S^{-2}/S_n^{-2}.[118] Polyurethane have

often been used as matrices for the preparation of ionomers and of polymer electrolytes.[119] The electrical conductivity of polyurethane can be enhanced by inserting the polar group such as sulfonate moieties in their polymer chain[112], which also facilitates the electrical conductivity of polyurethane. The cosensitized structure of QDs can provide better ability for effective charge injection from QDs to TiO_2[120] and the light absorption range becomes broader as compared to single QDs such as CdS and CdSe.[121] Due to high extinction coefficient, tunable band gap[122] and better photostability[16] of QDs, most of the researcher used cosensitized QDs photoelectrode in QDSSCs. Our assumption is to develop polymer gel electrolytes as a better hole transport agent and the fabricated device shows the high efficiency with performance stability.

In this chapter, functionalized thermoplastic polyurethane has been developed as gel electrolyte and hole transport materials in quantum dot sensitized solar cell. Gel electrolyte based QDSSCs is fabricated using cosensitizer like TiO_2/CdS/CdSe as photoelectrode. The redox couple electrolyte is used to transport holes to counter electrode. To overcome the limitation of liquid electrolytes, introduction of functionalized thermoplastic polyurethane polymer gel electrolytes in QDSSCs has improved the quality of the device together with the efficiency.

3.2 Results and Discussion

3.2.1 Attachment of Pendant Group and its Interaction with Polyurethane Chain

The synthetic process and functionalization of polyurethane is shown **Scheme 1,** where MDI and PTMG based prepolymer further react with butane diol in presence of catalyst to form long chain polyurethane. Subsequently, polyurethane is reacted with propane sultone to attach extended sulfonate group in the main chain to introduce ionic character in hydrophobic polyurethane.

The NMR spectra of PU and SPUs polymer with various degree of sulfonation are shown **in Fig 3a**. The corresponding spectra of pure and functionalized PU reveals a gradual increase in the intensity of the peaks at 8.53 ppm (leveled at 1) due to sulphonate proton and another three new

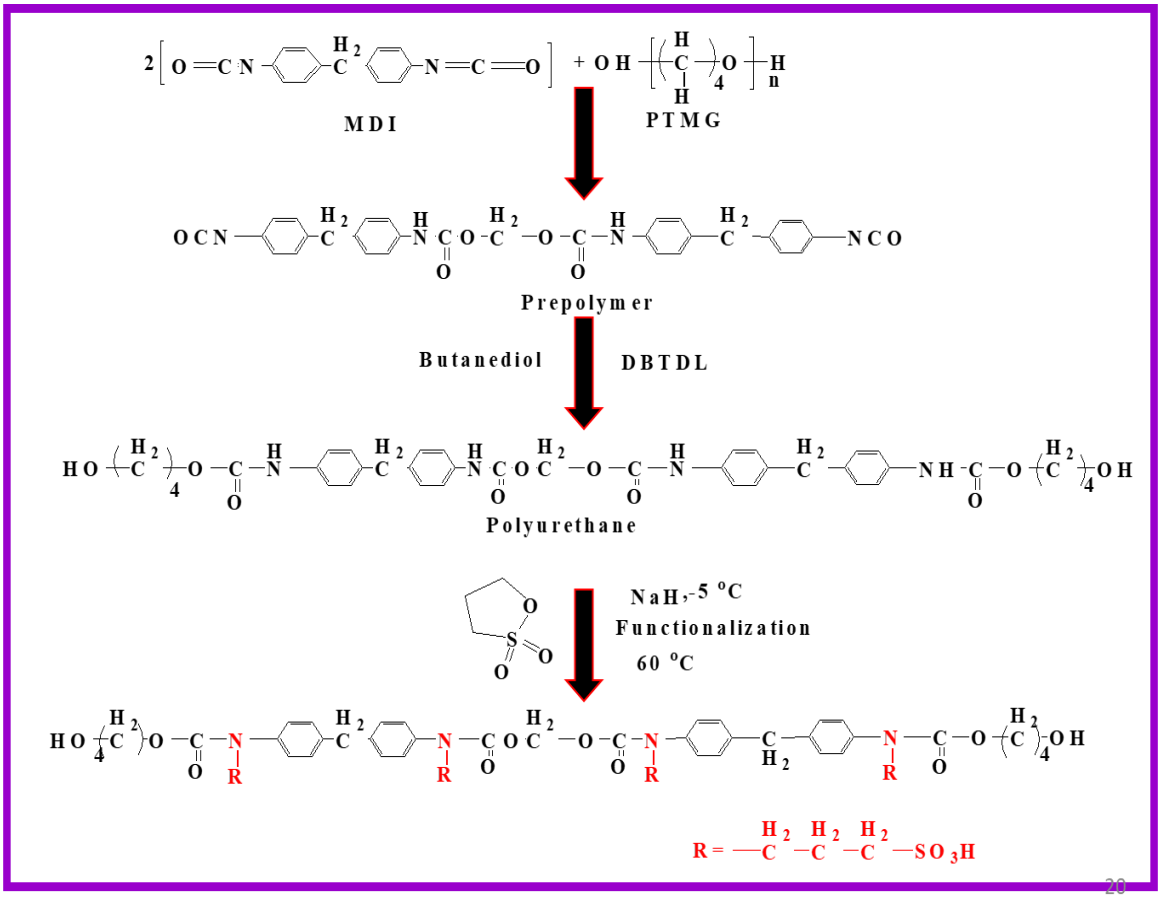

Scheme 3.1: The synthesis of the pure polyurethane and its subsequent.

peaks at ~ 4.5 ppm, 1.9 ppm and 1.5 ppm (levelled at 2, 3 & 4) for -CH_2 proton[123,124] in functionalized polymer with increasing the degree of sulphonation, which indicate that the attachment of sulphonate group in polymer chain from propane sultone.[115,125]

The degree of sulfonation was determined by using the relative intensity of all these characteristics peaks in SPU polymer. The degree of sulfonation was calculate by using the following equation[126],

$$DS\ (\%) = \frac{b/2}{a+a/2} \times 100 \qquad \text{.....3.1}$$

where, a is the peak area corresponding to the >NH group and b is the peak area of the signal corresponding to hydrogen atom $–CH_2$ group of propane sultone. The degree of sulfonation was observed for SPU-1, SPU-2, SPU-3 and SPU-4 polymer are 18, 42, 58 and 81% upon continuous substitution of hydrogen atom at urethane linkage. The **Fig 3.1b** represent the plot of degree of sulfonation as a function of weight ratio of the sulfonating agent to the urethane linkage of PUs, and we observed that degree of sulfonation was increased with increasing the amount of propane sultone.

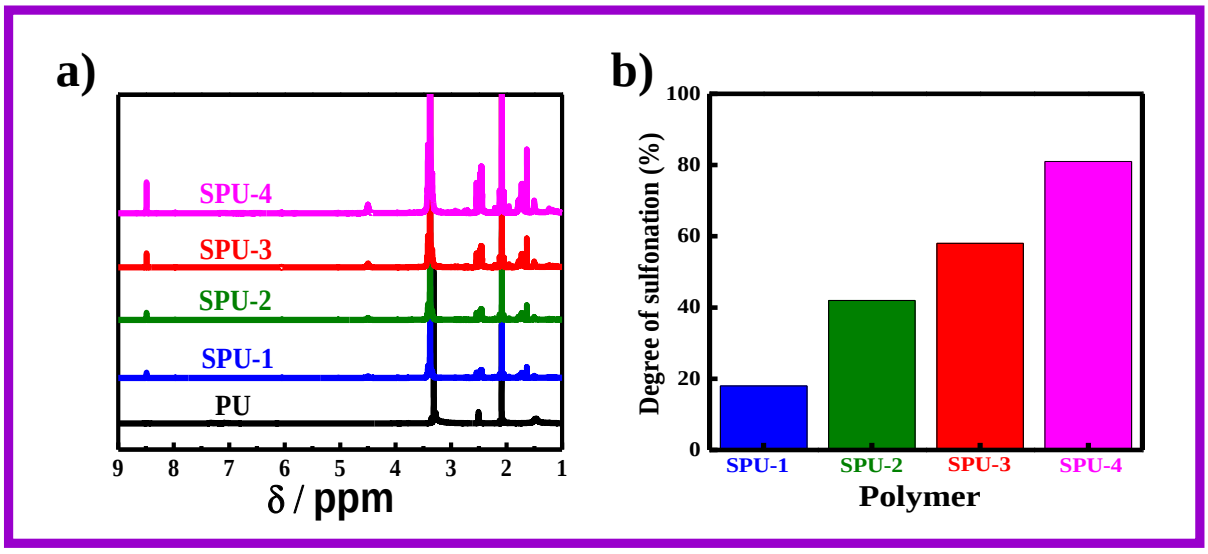

Figure 3.1: (a) ^{1}HNMR spectra of pure and various functionalized PUs **(b)** degree of sulfonation as a function of the sulfonating agents.

The FTIR spectra of pure and sulfonated polyurethane was another support of the evidence of the successful attachment of sulfonated group in polymer chain of polyurethane which are shown in **Fig 3.2 a**. From the FTIR spectra of pure and sulfonated PUs we observed that the shifting of >NH vibration peaks in pure PU at 3307 cm^{-1} to 3444 cm^{-1} (SPU-4) in higher degree of sulfonation is due to intermolecular hydrogen bonding between sulfonate group and >NH moieties.[127,128] The >NH vibration peaks are shifted at 3373 cm^{-1}, 3398 cm^{-1}, 3414 cm^{-1} and 3444 cm^{-1} for SPU-1, SPU-2, SPU-3 and SPU-4 sulfonated polyurethane respectively. And another new peak was observed at 1173 cm^{-1}, 1179 cm^{-1}, 1183 cm^{-1} and 1194 cm^{-1} in SPU-1, SPU-2, SPU-3, and SPU-4 respectively, which is absent in pure polyurethane.

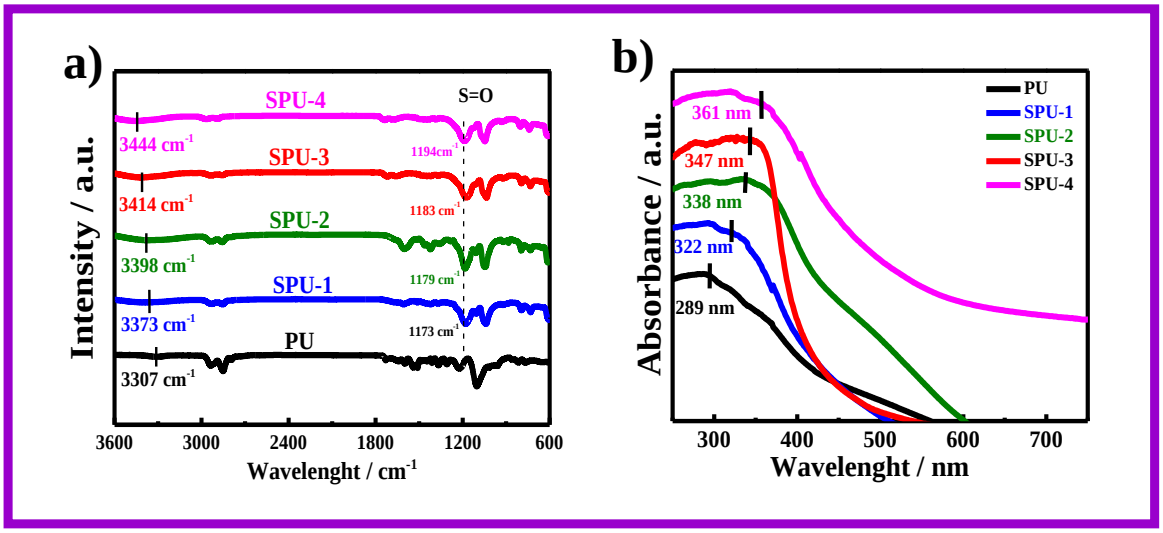

Figure 3.2: (a) FTIR measurements of pure and various degree of functionalized PUs (b) UV-vis spectroscopy measurements of pure and functionalized PUs.

The UV-Vis absorption spectroscopy of pure and sulfonated polyurethane polymers was shown in **Fig 3.2 b**. Pure PU shows a peak at 288 nm due to n → π* transition[129], while 322, 338, 347, and 361 nm broad peaks are noticed in the functionalized polymers of SPU-1, SPU-2, SPU-3, and SPU-4, respectively, predominantly from the sulfonate groups (n → π* transition).It is interesting to mention that absorption capability of the entire UV and partial visible region up to 450 nm has significantly gone up from the functionalized PUs as compared to pure PU, which in turn enhances the light harvesting capacity, suitable for solar cell application. Further, the absorption peak gradually shifts toward a higher wavenumber for a greater degree of sulfonation and this red shift is the indication of a better interactive system through specific interaction. However, the shifting of absorption peaks toward the visible region for higher sulfonated PUs indicates the size quantization effect.

3.2.2 Thermal Stability of Polyurethane Ionomer

The thermal stability of PU and functionalized PU has been verified through thermogravimetry by measuring the weight loss as function of temperature. The two-step degradation is prominent both in PU and SPU-3, while lower degradation is noticed in functionalized PU (SPU-3) because of early degradation of sulfonate group as reported earlier **(Figure 3.3 a).** Weight loss at low temperature is due to early degradation of the hard segment of the PU chain while high-temperature weight loss occurs because of degradation of the soft segment. Slight initial weight loss in SPU-3 arises because of loss of adsorbed moisture, which arises because of the hydrophilic nature of functionalized PU. Differential thermal analysis (DTA) curves of the sample quantitatively indicate the inflection point of the degradation temperature, and 258 °C is measured for SPU-3 against 320 °C for pure PU **(Figure 3.3 b).** The peaks at the higher temperature appear because of

the degradation of the soft segment in DTA profiles. The melting temperature of pure PU is measured to be 11 °C, while a considerably higher melting temperature of ~48 °C is noticed in SPU-3 presumably because of greater interaction arising from the ionic sulfonate moiety with the polar >N−H group in the hard segment of PU **(Figure 3.3 c).**

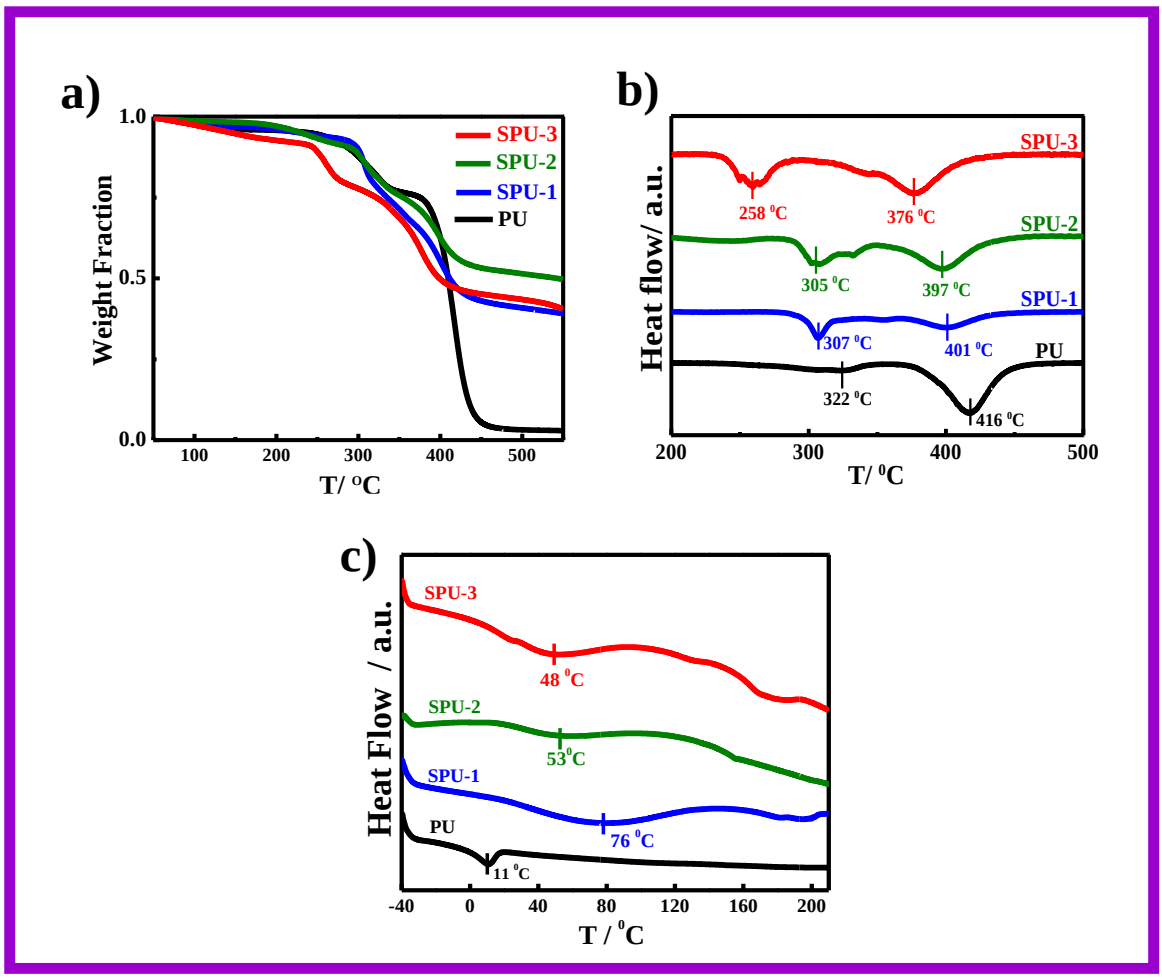

Figure 3.3: (a) TGA thermograms of pure and functionalized PUs (b) DTA of pure and functionalized PUs (c) DSC measurements of pure and functionalized PUs.

3.2.3 Electrochemical Analysis and Measurements of Polyurethane Ionomer

It is important to know whether the materials developed for the solar cell are corrosive or not, keeping the durability of the cell in mind. The effect of the materials as inhibitors on the cathodic and anodic reactions is estimated from potentiodynamic polarization measurement with a three-electrode setup, mild steel as the working electrode, Ag/AgCl as a reference electrode, and platinum as the counter electrode.[130] The working electrode of the dimension $3 \times 1 \times 0.1$ cm^3 under the active area is 1 cm^2 is dipped in acid solution. The linear Tafel plots of the anodic and cathodic (I−V characteristic) curves are extrapolated up to their intersection point to find out the corrosion current densities (I_{corr}) and corrosion potential (E_{corr}).[124] The inhibitor efficiency is calculated from measured I_{corr} values using the following equation

$$IE\ \% = \frac{I^0_{Corr} - I_{Corr}}{I^0_{Corr}} \times 100 \qquad \text{.....3.2}$$

where, I^0_{Corr} and I_{corr} are current densities without and with the presence of inhibitors, respectively. The linear polarization Tafel plots are shown in **Figure 3.4 a.** In case of a blank coupon (without inhibitor), the I_{corr} and E_{corr} are found to be 0.02548 A/cm^2 and 0.445 V, respectively. The corrosion current density decreased significantly using 50 ppm concentration of the SPU-3 inhibitor and its value of I_{corr} = 0.001884 A/cm^2, and the corrosion potential shifted from −0.445 to −0.461 V with a measured inhibitor efficiency (η) of 25.94%. The variations of I_{corr} and E_{corr} with the concentration of the inhibitor are shown in **Table 3.1** which shows the gradual shift of the corrosion potential upon increasing the inhibitor concentration, and the extent of inhibition efficiency (η) of 82.5% is achieved using 500 ppm concentration of functionalized SPU-3 **(Figure**

3.4 b). However, the functionalized PU is found to be the corrosion inhibitor, and it is expected to be of greater durability of the solar cell using this material.

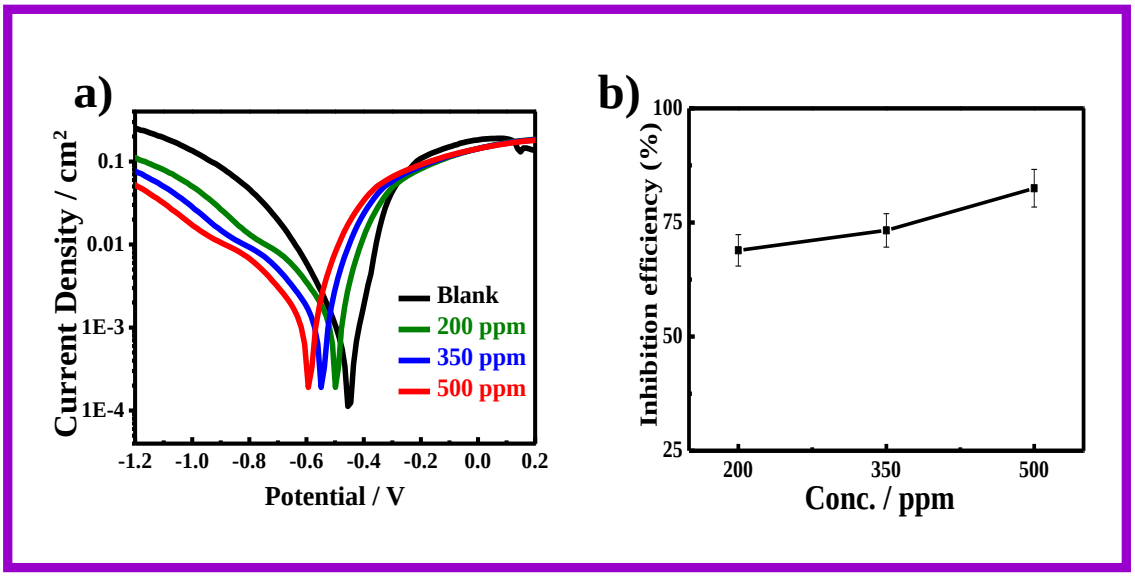

Figure 3.4: (a) Potentiodynamic polarization (I-V) measurements of mild steel with and without the inhibitor in 0.5 M H_2SO_4; (b) variation of percentage inhibition efficiency with inhibitor concentration

CV is an important technique to find out the information regarding electrochemical reactions that occur at the electrode−electrolyte interface.[131] CV is a potentiodynamic electrochemical technique commonly used to investigate the electrochemical properties of the analyte in solution, especially to estimate the current produced in the electrochemical cell in a potential range with specific scan rate**. Figure 3.5a** represents the current−potential curve for functionalized PUs from the CV measurement. The E_{OX} values are 0.96, 0.88, and 0.77 V for SPU-1 SPU-2, and SPU-3, respectively, and the E_{HOMO} values are measured to be −5.36, -5.28, and −5.17 eV using **eq 2.5**. The optical band gaps of functionalized polymers, calculated by using Tauc's plots (**Figure 3.5**

b), are 3.06, 2.96, and 2.83 eV for SPU-1, SPU-2, and SPU-3, respectively, and the optical band gap (Eg) of the sulfonated polymer decreased considerably upon increasing the degree of sulfonation.

Table 3.1: Corrosion Current Density, Potential, and Percentage Inhibition Efficiency of Functionalized PUs (SPUs) at Different Concentrations

Inhibitor	Inhibitor Concentration (ppm)	Corrosion potential (V)	Polarization resistance (Ω/cm^2)	Corrosion Current density (A/cm^2)	Inhibition efficiency (%)
Blank	-	0.445	5.304	0.02548	-
SPU-3	50	0.461	5.668	0.01884	25.94
SPU-3	100	0.466	7.052	0.01387	45.56
SPU-3	200	0.475	10.145	0.00792	68.91
SPU-3	350	0.531	10.82	0.00681	73.25
SPU-3	500	0.591	12.13	0.00445	82.50

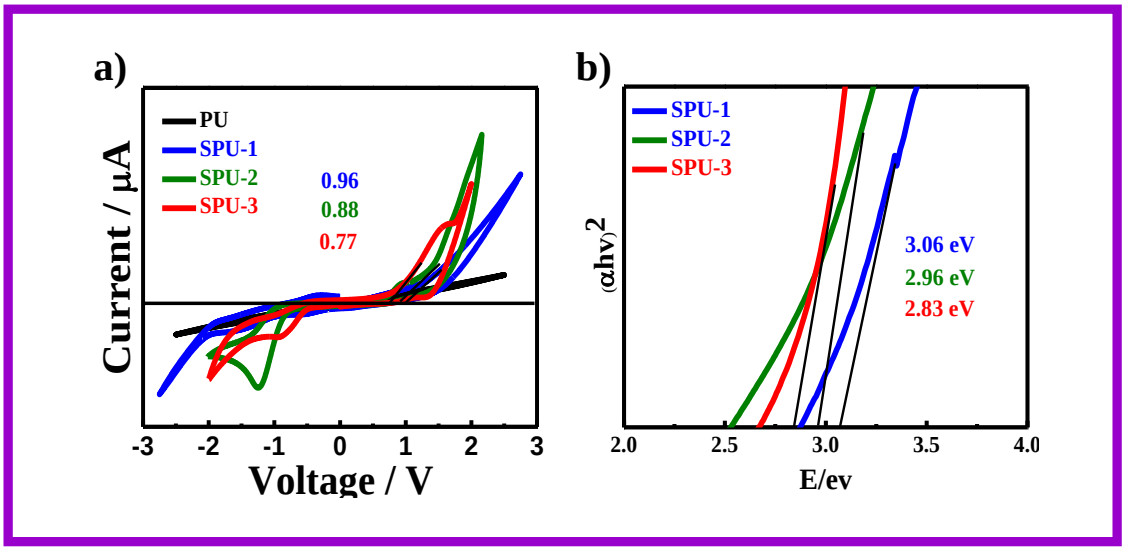

Figure 3.5: (a) CV measurements of indicated PU and functionalized PUs; (b) optical band gap of various functionalized PUs.

E_{LUMO} is estimated by using the optical band gap in **eq 2.6**, and E_{HOMO} value is obtained from CV measurement. Thus, the calculated values of E_{LUMO} of SPU-1 and SPU-3 are found to be −2.30 and −2.34 eV, respectively.

3.3 Quantum Dots synthesis, Quantum Confinements and its Optimization

3.3.1 Electrochemical Response of CdS and CdSe Quantum Dots

The CV patterns of CdS and CdSe are shown in **Figure 3.6 (a & b),** indicating the E_{OX} values of 0.50 and 0.57 V for CdS and CdSe, respectively. Subsequently, E_{HOMO} values of CdS and CdSe are measured to be −4.90 and −4.97 eV, respectively, while the E_{LUMO} values are calculated to be −2.67 and −2.81 eV. The optical energy band gap (E_g) of CdS, CdSe QD is calculated from UV−visible absorption spectra using Tauc's plots[132], $(\alpha h\nu)^2$ versus hν, indicating the E_g values of 2.23, and 2.16 for CdS, and CdSe respectively, in their bulk structure **(Figure 3.6 c)**.

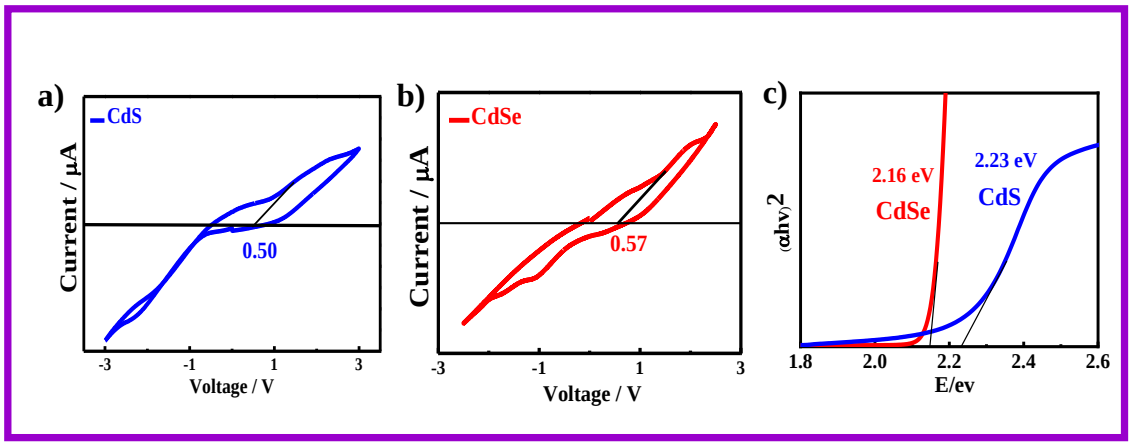

Figure 3.6: (a) CV measurements of CdS QDs; (b) CV measurements of CdSe QDs (c) optical band of CdS and CdSe QDs.

The optical energy band gap values and difference between VB and CB energy levels of QDs change slightly when they are in a layered structure on top of TiO_2, having 2.34 and 2.59 eV for CdS and CdSe, respectively, and the higher value of the band gap is explained from their interaction with TiO_2.

3.3.2 Particle Size Optical Response and its Interaction

A capping agent, EDTA, is used to synthesize QDs to avoid agglomeration. FTIR spectra of CdS and CdSe are shown in **Figure 3.7a**. A broad peak of EDTA-capped CdS at 3429 cm^{-1} is due to the O−H stretching frequency of water absorbed on the CdS surface attached through hydrogen bonding. A peak at 687 cm^{-1} in capped CdS is due to C−H stretching and bending mode, and it's shifting as compared to pure EDTA arises from the strong interaction between organic−inorganic moieties. Other major peaks at 1424 and 1045 cm^{-1} are assigned for the bending vibration of entrapped methanol used during synthesis. It is to mention that the above peaks do not appear in uncapped CdS, and, thereby, EDTA capping is confirmed through FTIR spectra. FTIR bands at 1461 and 1372 cm^{-1} in capped CdSe are assigned to antisymmetric and symmetric vibrations of the carboxylate anion (COO−), respectively, which indicate that carboxylic groups are bound to the Cd surface of CdSe QDs. Intense peaks at 2918 and 2850 cm^{-1} of CdSe QDs are due to antisymmetric and symmetric C−H stretching vibrations of the -CH_2 group,[133] and the absence of the stretching vibration at ∼1700 cm^{-1} is the indication of the absence of oleic acid, which is removed during the washing process. The absorption spectra of synthesized QDs (CdS and CdSe) are shown in **Figure 3.7b**, which confirm the formation of CdS and CdSe QDs. The first excitonic

absorption peak of the as-prepared QDs in the visible region and the absorption edge occurs at 495 and 538 nm for CdS and CdSe QDs, respectively.

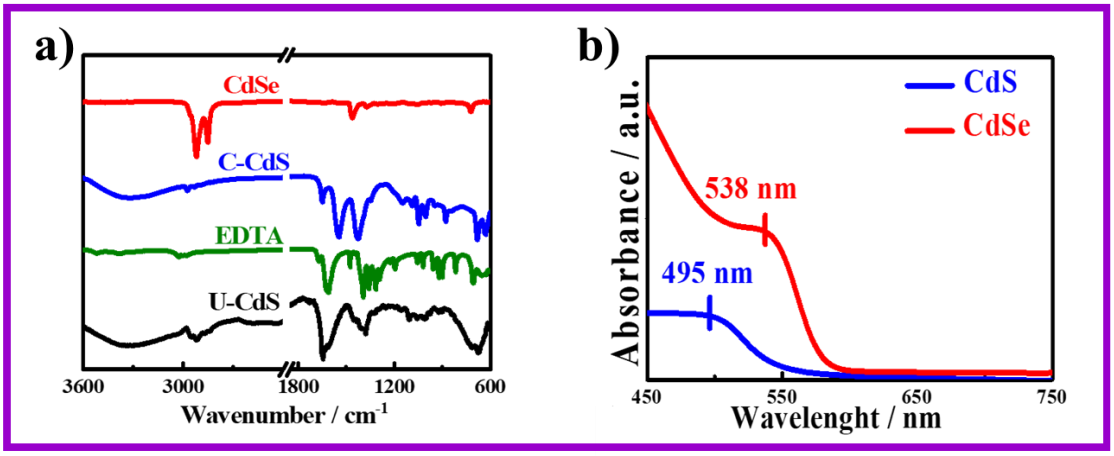

Figure 3.7: (a) FTIR spectra of synthesized CdS and CdSe (b) UV-visible spectra of CdS and CdSe QDs

Transmission electron microscopy (TEM) bright-field images are taken to understand the formation of QDs and an average particle size of 5 and 4 nm for CdS and CdSe QDs, respectively **Figure 3.8**(a & b). Almost spherical particles are noticed with moderate particle size variation, as shown in the inset bar diagram of individual TEM images.

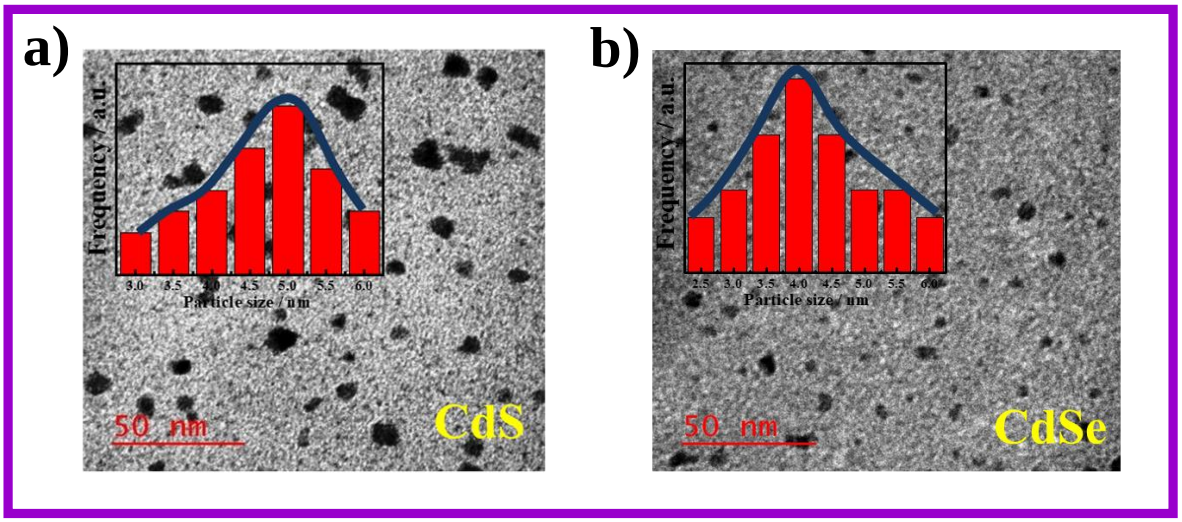

Figure 3.8: (a) TEM bright-field image and particle size distribution of CdS in the inset (b) TEM image and particle size distribution of CdSe QDs.

3.4 Fabrication of QDSSCs and its Photovoltaic Conversion Efficiency

3.4.1 Light Harvesting Efficiency, Energy Profile Diagram and Photovoltaic Reaction

Both QDs and functionalized polymers are developed for solar cell application, and now, it is important to know the light harvesting capability of the materials. Similar to the fabrication of the solar cell, the materials are deposited layer by layer, as shown in the inset of **Figure 3.9 a** showing the change in color of the transparent FTO/TiO_2 electrode into yellow after the deposition of CdS QDs. Further change in color to orange is observed after loading of CdSe QDs over the CdS layer.

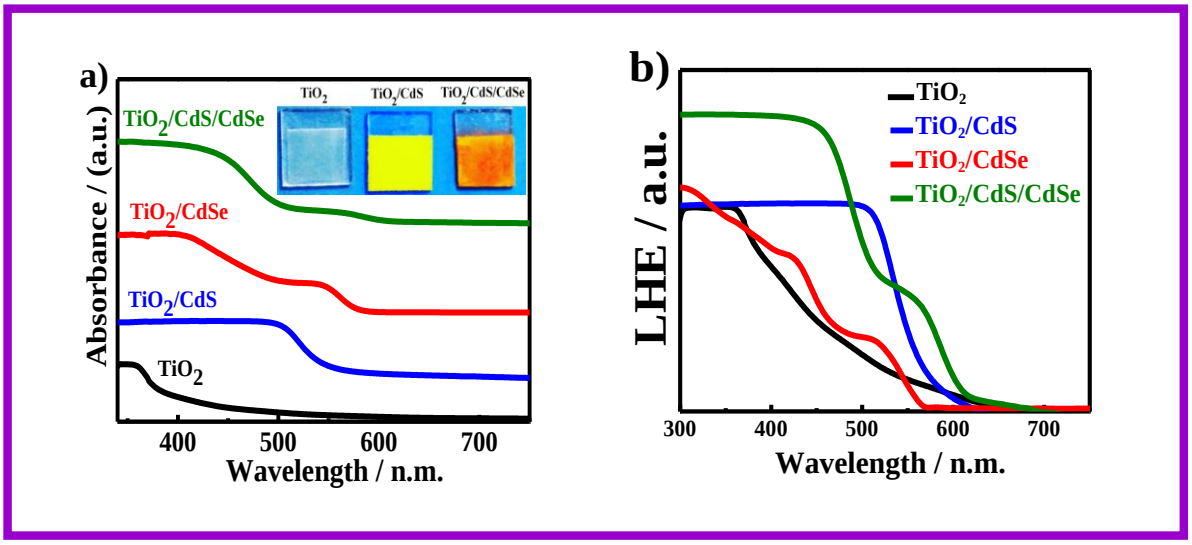

Figure 3.9: (a) UV-visible absorbance spectra of FTO/TiO_2, FTO/TiO_2/CdS, and FTO/TiO_2/CdS/CdSe; (b) light harvesting efficiency of photoanode (FTO/TiO_2, FTO/TiO_2/CdS, and FTO/TiO_2/CdS/CdSe).

UV−visible absorption spectra of pure TiO_2, TiO_2/CdS, TiO_2/CdSe, and TiO_2/CdS/CdSe electrodes are shown in **Figure 3.9a,** and a broader absorption band is evident in the TiO_2/CdS/CdSe electrode as compared to single TiO_2/CdS and TiO_2/CdSe electrodes, indicating the cosensitization effect of solar light absorption. Thus, the fabricated cosensitized TiO_2/CdS/CdSe photoanode suggests the improvement of light absorption and is favorable for capturing more photons, which in turn can produce more excitons. The light harvesting efficiency is calculated using following eq 3.3 (**Figure 3.9b**).

$$LHE = 1 - 10^{absorbance} \quad \text{.....3.3}$$

On combining the energy levels from the band gap (E_g), E_{HOMO} and E_{LUMO} from CV measurements **(Figure 3.5 a & b and Figure 3.6 a, b &c),** an energy profile diagram has been drawn to understand the suitability of electron and hole transport from QDs to polymers/anode electrode and **Figure 3.10** represents comparative band energy diagram of functionalized SPU-1 and CdSe quantum dots, SPU-2 and CdSe quantum dots, and SPU-3 and CdSe quantum dots are shown in Figure 3.10(a, b and c) respectively.

.

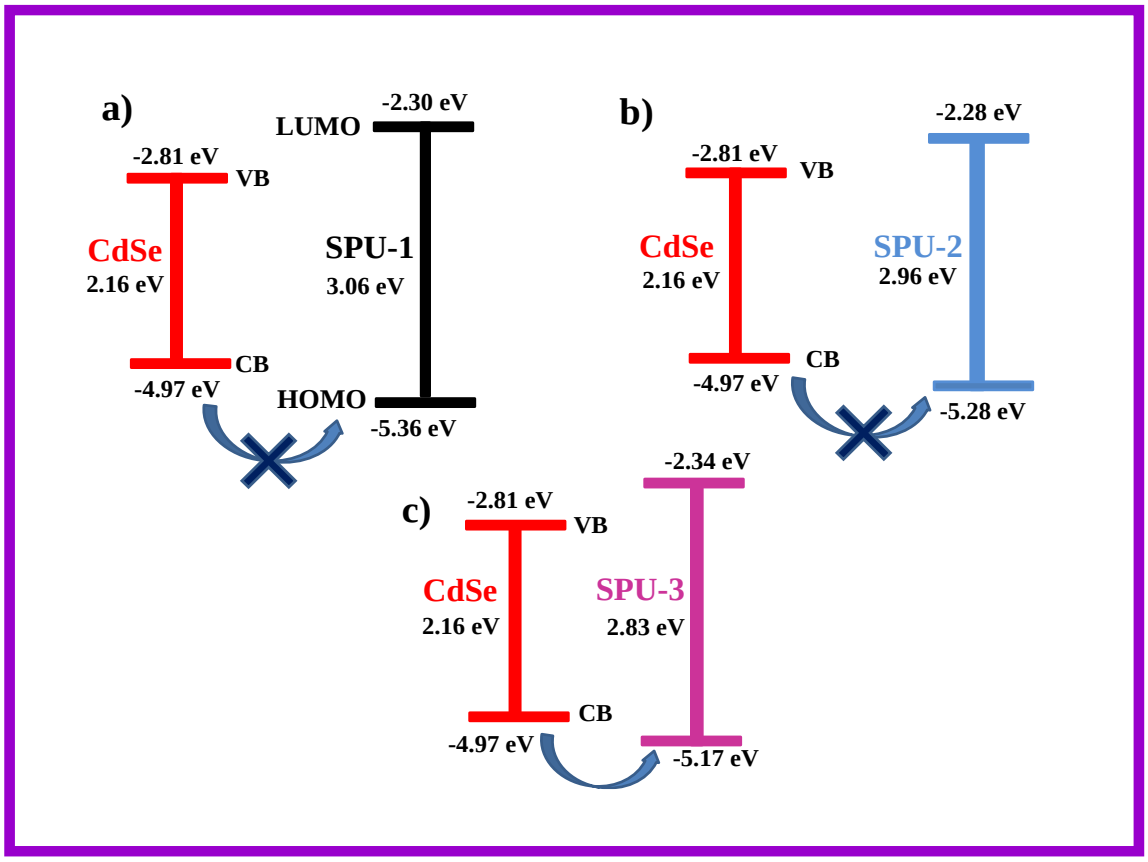

Figure 3.10: (a) comparative band energy diagram of functionalized SPU-1 and CdSe quantum dots; (b) comparative band energy diagram of functionalized SPU-2 and CdSe quantum dots; (c) comparative band energy diagram of functionalized SPU-3 and CdSe quantum dots.

From the above diagram (**Figure3.10**) we calculated that the energy difference between CB of CdSe QDs and EHOMO level of the SPU-1, SPU-2 and SPU-3 sulfonated polymer are 0.39, 0.31 and 0.20 respectively. The difference between CB of CdSe QDs and SPU-3 are very close together as compared to other sulfonated polyurethane, hence holes are easily transport to the EHOMO level of SPU-3 from to CB of CdSe QDs. The suitable band energy diagram is shown in **Figure 3.11a.**

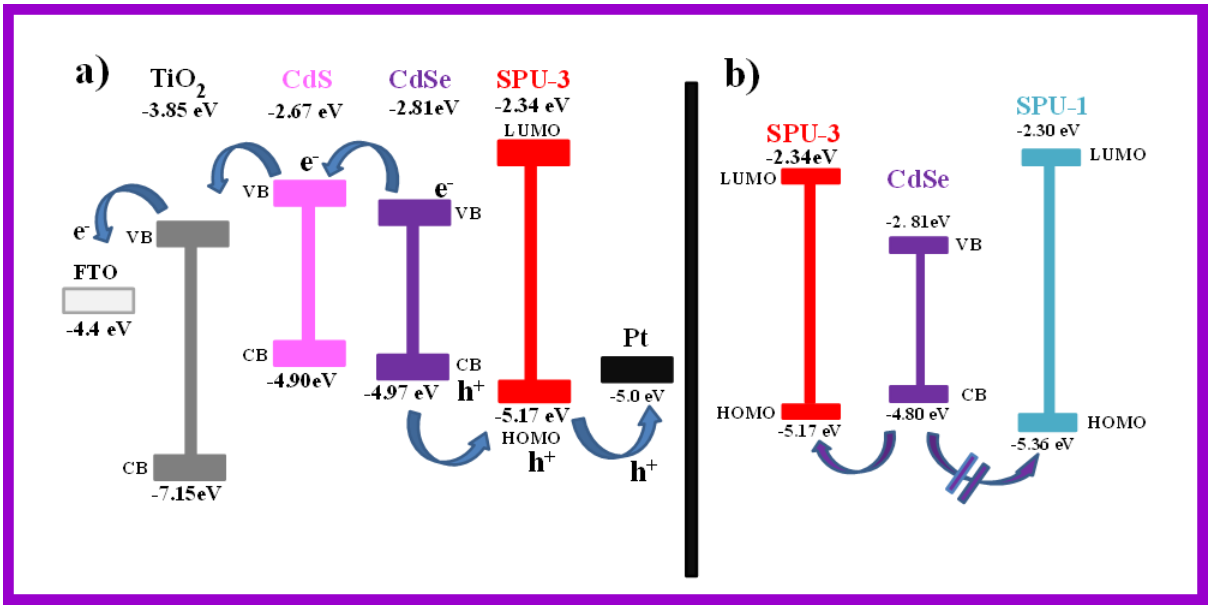

Figure 3.11: (a) Energy profile diagram of TiO_2, CdS, and CdSe QDs with SPU-3 gel electrolytes with energy levels as calculated from E_g, E_{HOMO}, and E_{LUMO}. The arrow indicates the flow of excitons under a suitable energy level; (b) comparison of the energy level of the SPU polymer with CdSe QDs showing difficulty n transport of the holes.

The excitons (electron−hole pairs) are generated after the absorption of photons by CdSe QDs, and the excited electrons can easily transport to the conduction band of CdS QDs rather than LUMO

of SPU-3 because of the meager energy difference (0.14 eV) between the conduction band of both CdS and CdSe, and there is quite large difference in energy level value with the LUMO level of SPU-3 (0.47 eV) **(Figure 3.11a)**. Similarly, the holes in CdSe can transport easily to the HOMO level of SPU-3 from the valence band, understanding the close proximity of the energy levels.

3.5 Hole Transportation, Redox Reaction and PCE of QDSSCs

The mismatch in the CdSe QDs and other functionalized PU (SPU-1) has been shown in **Figure 3.10b**, raising the importance of proper functionalization of thermoplastic PU for better exciton transport for possible solar cell applications. The chances of exciton recombination would be high in case of SPU-1 and SPU-3, which is justified for better performance using the TiO_2/CdS/CdSe cosensitized photoanode with SPU-3 gel electrolyte QDSSC. The solar cell has been devised using the developed photoanode and functionalized polymer gel electrolyte. The complete array has been shown in **Figure 3.12a** and the layer-by-layer deposition to construct photoanode is shown in **Figure 3.12b**. The photocurrent−voltage characteristic curves of the various photoelectrodes, TiO_2/CdS, TiO_2/CdSe, TiO_2/CdSe/CdS, and TiO_2/CdS/CdSe of the QDSSCs with the prepared polymer gel electrolyte (SPU-3) under solar radiation (AM 1.5G) with a light intensity of ∼100 mW/cm^2 are shown in **Figure 3.12c**. The open-circuit voltage (Voc) and FF for the cosensitized photoanode (TiO_2/CdS/CdSe) is found to be the highest (0.74 V). The relative efficiency in TiO_2/CdSe is noticed to be considerably higher in terms of photocurrent density than TiO_2/CdS as the photoanode. It is interesting to note that the TiO_2/CdSe/CdS photoanode, prepared through reversal of the deposition of layers but keeping the other parameters, such as the method, thickness, and so forth, exhibit a very low open circuit voltage (0.22 V) and photocurrent density (2.91

mW/cm^2), primarily because of the mismatch of the energy level, as shown in **Figure 3.11(a-c).** The power density has been plotted as a function of potential in **Figure 3.12d**, showing the variation of generated power from the solar simulator.

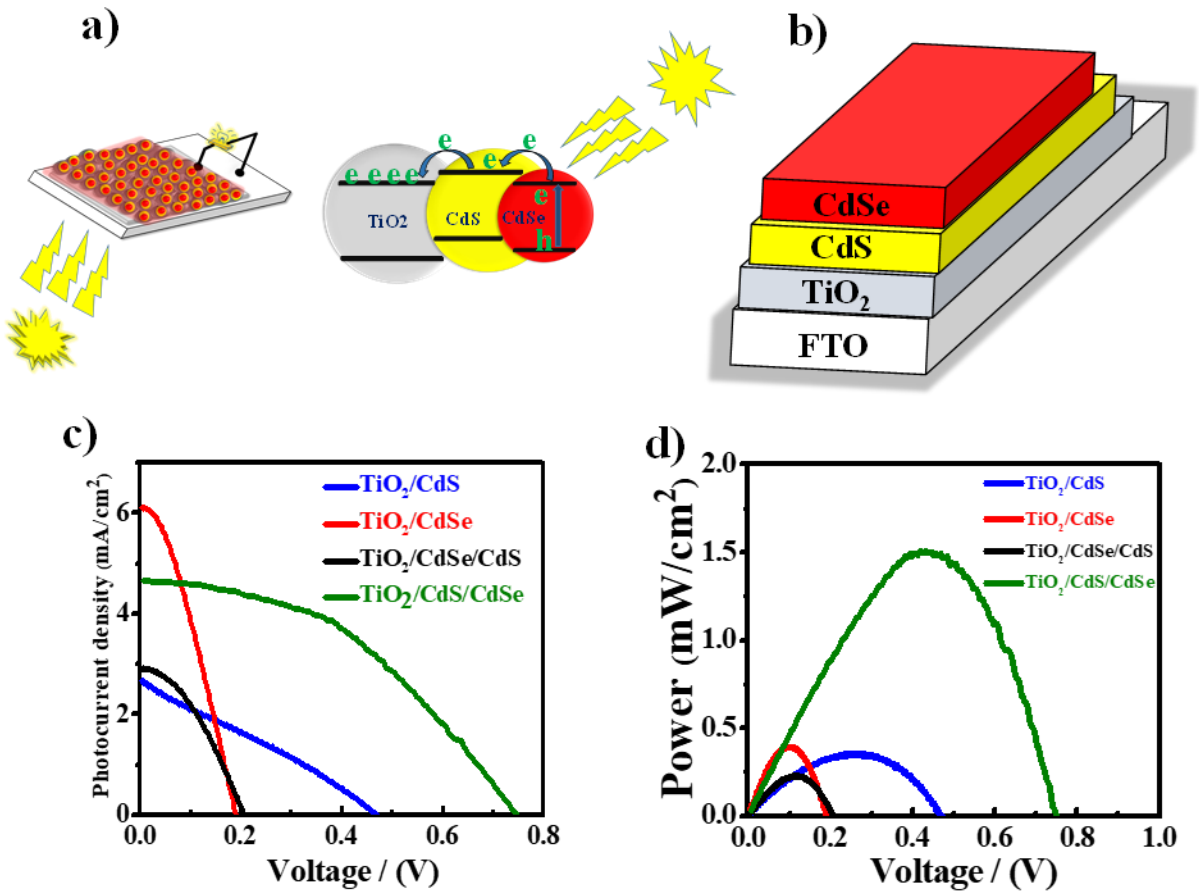

Figure 3.12: (a) Array of the photoanode and solar excitation mechanism for the constructed solar cells; (b) layer by layer deposition of TiO2, CdS, and CdSe to fabricate the photoanode; (c) J-V characteristics measurements to calculate the photocurrent density and open circuit voltage under 1-sun illumination (100 mw/cm2); (d) power voltage curve to calculate the PCE of the indicated QDSSCs.

The short-circuit current density (Jsc), open-circuit voltage (V_{oc}), FF, and PCE (η) of these cells having different architecture are presented in **Table 3.2**. The cosensitized TiO_2/CdS/CdSe photoelectrode shows the highest PCE (η = 1.51%) with an FF of 0.44 and open circuit voltage (Voc) of 0.74 V, and short-circuit current density (Jsc) of 4.66 mA/cm^2 as compared to individual TiO_2/CdS- or TiO_2/CdSe-sensitized photoelectrodes. This superior efficiency in the cosensitized system is due to the combination of CdS and CdSe QDs, which have complementary effect in light harvest as discussed above, and the stepwise band-edge level structure of CdS/CdSe QDs, which facilitate the rate of electron ejection from CdSe QDs and excited electron transports from CdS QDs to TiO_2.This is to note that considerably low PCE (η) of 0.36% is observed for an individual photoanode such as TiO_2/CdS and using the configuration of TiO_2/CdS/SPU-3 arises from its low FF (0.29 V), poor circuit current density (Jsc) of 2.66 mA/ cm^2, and open circuit voltage (Voc) of 0.46 V.

Table 3.2: Short-circuit Current Density (Jsc), Open-circuit Voltage (Voc), FF, and PCE (η) of Various Cells Using the Indicated Photoanode and SPU-3 Polymer Gel Electrolytes

Photoanode	$J_{sc\ (mA/cm^2)}$	$V_{oc\ (volt)}$	Fill Factor	Efficiency
TiO_2/CdS	2.66	0.46	0.29	0.36
TiO_2/CdSe	6.09	0.20	0.33	0.40
TiO_2/CdSe/CdS	2.91	0.22	0.36	0.23
TiO_2/CdS/CdSe	4.66	0.74	0.44	1.51

The TiO_2/CdSe photoelectrode exhibits slight better performance of PCE (η = 0.40%) than the TiO_2/CdS electrode from its better short-circuit current density (Jsc) of 6.09 mA/cm^2, presumably because of the broader light absorption coefficient of CdSe QDs, as opposed to CdS.

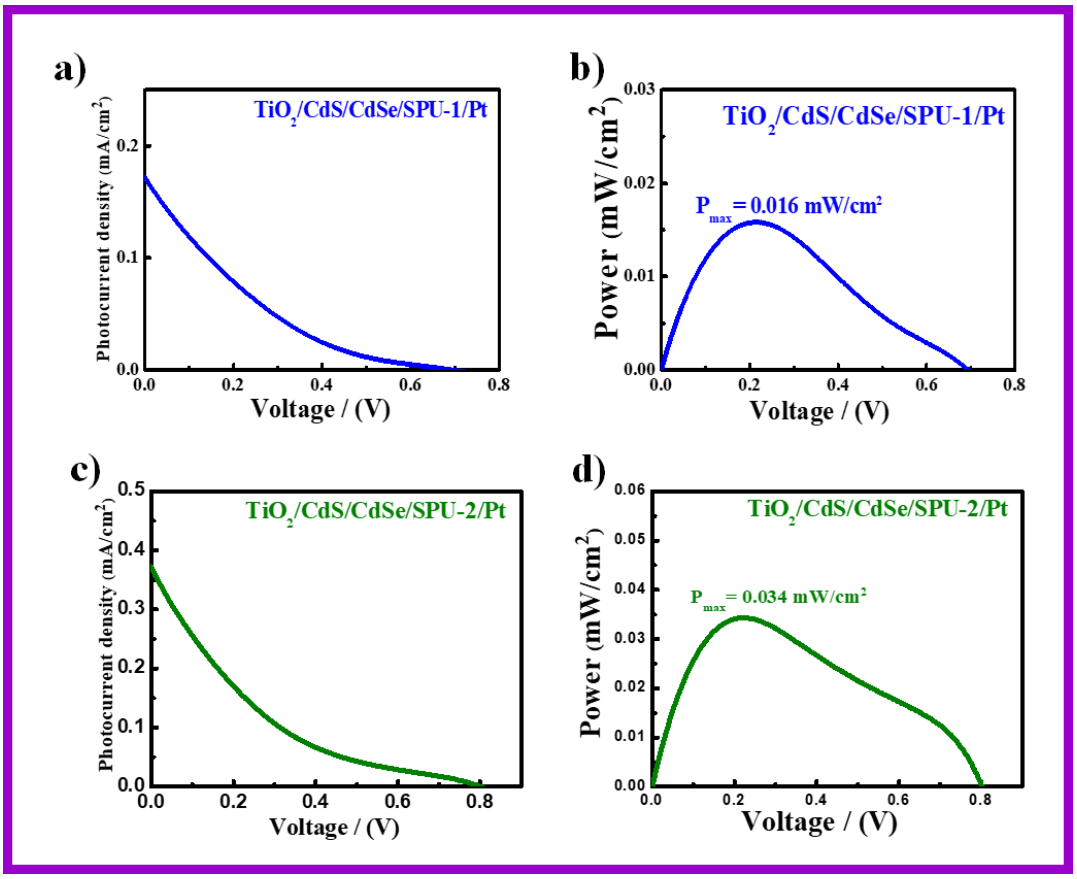

Figure 3.13: (a) represent the photocurrent density-potential curve using the SPU-1 gel electrolyte with TiO_2/CdS/CdSe photoanode; (b) represent the power-voltage (J-V) curve using the SPU-1 gel electrolyte with TiO_2/CdS/CdSe photoanode; (c) represent the photocurrent density-potential curve using the SPU-2 gel electrolyte with TiO_2/CdS/CdSe photoanode; (d) represent the power-voltage (J-V) curve using the SPU-2 gel electrolyte with TiO_2/CdS/CdSe photoanode.

Hence, a cosensitized system is much efficient than a single electrode material. Similarly, a cell has been constructed using the optimized photoanode (TiO_2/CdS/CdSe) and SPU-1 with a lower degree of sulfonation, which shows 0.034% PCE, and the details have been presented in **Figure 3.13(a-d)**. The polymer gel electrolyte acts as a hole-transporting agent, and its higher degree of sulfonation helps to carry the holes to the Pt electrode and, thereby, favoring the cell efficiency using SPU-3 as the electrolyte. This is to mention that there is an optimum sulfonation level beyond which the functionalized PU becomes liquid and can no longer be used for safe and durable application. Thus, suitable polymer gel electrolytes and proper layering of photoanode provide the required high PCE using sunlight.

3.6 Conclusion

Our strategy is to develop the thermoplastic polyurethane gel electrolytes as a hole transport material in quantum dots sensitized solar cells. A wide range of HOMO and LUMO energy levels are generated in gel electrolyte materials, depending on the extent of functionalization, as measured through CV and optical band gap measurement using light absorption studies. The prepared polymer gel electrolyte blocks the electron flow and thereby reduces the recombination of interfacial charges, reduces the leakage problem, increases the built-in potential of the device, and significantly enhances the open-circuit voltage (Voc) of the device. QDs of CdS (5 nm) and CdSe (4 nm) as sensitizers have been synthesized having varying dimensions using capping agents to avoid agglomeration of particles. Light harvesting efficiency of the TiO_2/CdS/CdSe photoanode, prepared through layer-by-layer deposition, is found to be significantly high using the cosensitized system. The band diagram of the QDs/sensitizers has been measured using absorption spectra (Tauc's plot) and CV. The solar cell device has been fabricated using the optimized photoanode

(TiO_2/CdS/CdSe) and 58% of degree of sulfonation (SPU-3), which exhibits a considerably high efficiency of 1.5% energy conversion using functionalized thermoplastic PU as the hole transport carrier. The limitation of the experimental work is to fabricate and measure the device performance in inert atmosphere.